

THE INFRARED PROPERTIES OF SUBMILLIMETER GALAXIES: CLUES FROM ULTRADEEP 70 μm IMAGING

MINH T. HUYNH

Spitzer Science Center, California Institute of Technology, Pasadena, CA; mhuynh@ipac.caltech.edu

ALEXANDRA POPE

Department of Physics and Astronomy, University of British Columbia, Vancouver, BC, V6T 1Z1, Canada

DAVID T. FRAYER

Spitzer Science Center, California Institute of Technology, Pasadena, CA

AND

DOUGLAS SCOTT

Department of Physics and Astronomy, University of British Columbia, Vancouver, BC, V6T 1Z1, Canada

Received 2006 October 11; accepted 2006 December 18

ABSTRACT

We present 70 μm properties of submillimeter galaxies (SMGs) in the Great Observatories Origins Deep Survey (GOODS) North field. Out of 30 submillimeter galaxies ($S_{850} > 2$ mJy) in the central GOODS-N region, we find two with secure 70 μm detections. These are the first 70 μm detections of SMGs. One of the matched SMGs is at $z \sim 0.5$, and has S_{70}/S_{850} and S_{70}/S_{24} ratios consistent with a cool galaxy. The second SMG ($z = 1.2$) has infrared-submillimeter colors that indicate it is more actively forming stars. We examine the average 70 μm properties of the SMGs by performing a stacking analysis, which also allows us to estimate that $S_{850} > 2$ mJy SMGs contribute $9\% \pm 3\%$ of the 70 μm background light. The S_{850}/S_{70} colors of the SMG population as a whole is best fit by cool galaxies, and because of the redshifting effects these constraints are mainly on the lower z subsample. We fit spectral energy distributions (SEDs) to the far-infrared data points of the two detected SMGs and the average low-redshift SMG ($z_{\text{median}} = 1.4$). We find that the average low- z SMG has a cooler dust temperature than local ultraluminous infrared galaxies (ULIRGs) of similar luminosity and an SED that is best fit by scaled-up versions of normal spiral galaxies. The average low- z SMG is found to have a typical dust temperature $T = 21\text{--}33$ K and infrared luminosity $L_{8\text{--}1000\ \mu\text{m}} = 8.0 \times 10^{11} L_{\odot}$. We estimate the AGN contribution to the total infrared luminosity of low- z SMGs is less than 23%.

Subject headings: galaxies: evolution — galaxies: formation — galaxies: starburst — submillimeter

1. INTRODUCTION

Deep submillimeter surveys provide a probe of galaxies that is almost independent of luminosity for a wide redshift range $1 < z < 5$ because of the negative K -correction in the infrared (e.g., Blain et al. 2002). The Submillimeter Common User Bolometer Array (SCUBA; Holland et al. 1999) and Max-Planck Millimeter Bolometer (MAMBO; Kreysa et al. 1998) have now discovered several hundred submillimeter galaxies (SMGs; e.g., Smail et al. 1997; Hughes et al. 1998; Barger et al. 1998; Borys et al. 2002; Chapman et al. 2002; Webb et al. 2003; Greve et al. 2004; Pope et al. 2005; Coppin et al. 2006). Our knowledge of SMGs has been hampered by the large beam size of the submillimeter telescopes, which makes it difficult to identify counterparts in the optical and near-infrared. For example, in the Great Observatories Origins Deep Survey (GOODS) North field there are typically ~ 10 *Hubble Space Telescope* Advanced Camera for Surveys (*HSTACS*) optical galaxies within a single SCUBA $15''$ beam.

Deep radio surveys have proven to be one of the best ways to identify the counterparts to SMGs (e.g., Ivison et al. 2000; Barger et al. 2000; Pope et al. 2006). The star formation processes that heat the dust responsible for the submillimeter light also produce radio emission, as evidenced by the well-known far-infrared–radio correlation. Taking advantage of this, SMGs have been matched to radio sources, which have much better positional accuracy, and the optical/near-IR counterparts can then be found after the radio

identification has been made. This is possible because the density of sources in the deepest radio images is much less than that of optical galaxies, so the probability of a chance coincidence is lower.

The current knowledge of SMGs is biased toward the radio-identified sources. The SMGs have a median redshift of about 2.2 and bolometric infrared (IR) luminosities $L_{\text{IR}} > 10^{12} L_{\odot}$ (Chapman et al. 2004, 2005). The optically identified SMGs are faint optically ($i_{775} \gtrsim 22$) and red ($i_{775} - K_s \simeq 2.3$ in AB magnitudes), with about 30% having colors consistent with extremely red objects (EROs; Pope et al. 2005). Thus, SMGs are thought to be high-redshift, dusty analogs of local ultraluminous infrared galaxies (ULIRGs).

The spectral energy distributions (SEDs) of SMGs have traditionally been fit with local ULIRGs as templates, and in particular Arp 220 (e.g., Barger et al. 2000), which has an effective dust temperature of about 42–47 K (Klaas et al. 1997; Dunne et al. 2000). Chapman et al. (2005) found a typical dust temperature of 36 ± 7 K and a median $L_{\text{IR}} = 8.5 \times 10^{12} L_{\odot}$ for their SMG sample. This is cooler than local ULIRGs, which have an average dust temperature of 43 ± 6 K (based on the Dunne et al. 2000 sample). The Far-IR Background (FIRBACK) study of 170 μm -selected galaxies found two ULIRGs in the range $0.5 < z < 1$ that have SEDs cooler and less luminous than Arp 220 (Sajina et al. 2006). A 350 μm study of radio-detected SMGs found temperatures of 35 ± 3 K (Kovacs et al. 2006). Using the 24 μm imaging from the *Spitzer* Legacy Project GOODS, Pope et al. (2006)

securely identify 60% of SMGs in this field in the mid-infrared (MIR) and have tentative counterparts for another 34%. It was found that the observed MIR-submillimeter-radio SED of the SMGs peak at longer wavelengths than local ULIRGs and are best fit by models with temperatures of about 30 K (Pope et al. 2006). There is thus an emerging picture that SMGs are cooler than previously thought.

Dust temperature affects the inferred IR luminosity, and hence star formation rate (SFR), that is derived for these galaxies. Studies of SMGs have often assumed dust temperatures of 40 K (see Blain et al. 2002). A drop from 40 to 35 K in temperature decreases the IR luminosity by about a factor of 2. Better knowledge of the temperature of SMGs is thus crucial for more accurate luminosity estimates.

The advent of the *Spitzer Space Telescope* makes it possible to study the MIR and far-infrared (FIR) properties of SMGs in detail for the first time. At the median SMG redshift of $z \sim 2$, polycyclic aromatic hydrocarbon (PAH) and silicate features fall into the rest-frame wavelength of the 24 μm band. This can make it difficult to determine the total IR luminosities and to fit model SEDs well to the FIR, which does not always correlate with the MIR. The 70 μm band of the Multiband Imaging Photometer for *Spitzer* (MIPS) instrument is not affected by PAH or silicate features for redshifts less than about 3, while the 160 μm band is not affected at all. Moreover, these MIPS bands are closer to the FIR peak than the MIR data points used in previous studies. The longer wavelength MIPS bands should therefore be extremely useful for studying SMGs. The sensitivities and confusion limits at 70 μm make this feasible, but difficult, and hence only the deepest MIPS data are likely to lead to SMG detections.

In this paper we present a study of the FIR properties and SEDs of submillimeter galaxies using the deepest 70 and 160 μm data available for the GOODS-N field. In particular, we use the 70 and 160 μm data to check if the SEDs of distant SMGs are consistent with those of local ULIRGs.

We assume a Hubble constant of $71 \text{ km s}^{-1} \text{ Mpc}^{-1}$, together with matter and cosmological constant density parameters of $\Omega_M = 0.27$ and $\Omega_\Lambda = 0.73$ in this paper. We also use the notation S_{70} , S_{850} , $S_{1.4}$, etc. throughout for the flux densities at 850 μm , 70 μm , and 1.4 GHz.

2. THE SUBMILLIMETER SAMPLE

The SCUBA “supermap” of GOODS-N contains 35 robust 850 μm detections. Details of the data reduction and source extraction can be found in Borys et al. (2003) and Pope et al. (2005). This submillimeter image contains all publicly available SCUBA mapping data in this field taken up until 2004. Although 450 μm data were also taken, they unfortunately have essentially no constraining power. Of the 35 SCUBA sources, 33 have likely radio and/or *Spitzer* counterparts using the Very Large Array (VLA), Infrared Array Camera (IRAC), and MIPS 24 μm data in GOODS-N (see Pope et al. 2006). Thirty of these SCUBA galaxies are within the ultradeep 70 μm image area. SCUBA sources with low signal-to-noise ratios (S/Ns) may have true flux densities that are boosted by a factor that depends on the source brightness and the local noise in the SCUBA map, and can be estimated if the source counts are known (see, e.g., Coppin et al. 2005). Therefore, in this study we use the deboosted 850 μm flux densities given in Pope et al. (2006).

3. SPITZER 70 AND 160 μm OBSERVATIONS

The MIPS 70 μm observations were carried out during Cycle 1 of the General Observer program (*Spitzer* program ID 3325; Frayer et al. 2006b). The inner $10' \times 10'$ of GOODS-N was

mapped to a depth of 10.6 ks. The data were taken in the small-field photometry mode of MIPS with 10 s Data Collection Events (DCEs). Each Astronomical Observation Request (AOR) consisted of an eight-position cluster map, and the observations were completed with 12 AORs in total. In addition to our GO data, we used the MIPS Guaranteed Time Observers (GTO) data (program ID 81; Dole et al. 2004). These GTO data have an integration time of 600 s.

The raw data were processed off-line using the Germanium Reprocessing Tools (GERT, ver. S13.1), following the algorithms derived by the MIPS team (Gordon et al. 2005). Instrumental artifacts in the Basic Calibrated Data (BCDs) were removed using the filtering techniques adopted for the extragalactic First Look Survey (xFLS; Frayer et al. 2006a). The data were calibrated assuming an absolute flux calibration factor of 702 MJy sr^{-1} per MIPS-70 μm unit for stellar SEDs. The flux densities were multiplied by 1.09 to apply a galactic SED color correction. This assumes a power-law SED of the form $f_\nu \propto \nu^\alpha$ and $\alpha = -1$, but the color corrections are similar for $\alpha = 0$ to -3 . A more detailed discussion of the data reduction can be found in Frayer et al. (2006b).

The final image achieves a sensitivity of ~ 0.6 mJy rms, and we have cataloged 101 sources (over 120 arcmin^2) with $S_{70} > 2.3$ mJy ($S/N > 3\sigma$). We catalog a region slightly larger than the area of deepest coverage to include some relatively bright 70 μm sources and improve statistics. The source counts are presented in Frayer et al. (2006b), and a full catalog will be presented in M. T. Huynh et al. (2007, in preparation). The 70 μm image has a beam size of 18.5'' FWHM, and in the presence of Gaussian noise the 1σ positional error of sources is of order $0.5\theta_{\text{FWHM}}/(S/N)$, i.e., 3'' for the faintest sources.

The 160 μm observations of the GOODS-N region were taken as part of the MIPS GTO program in 2004. These data were taken in the scan mode of MIPS, and we applied the standard filtering techniques to the 160 μm BCDs similar to what was used for the xFLS (Frayer et al. 2006a). The data were calibrated using a factor of 44.7 MJy sr^{-1} per MIPS-160 μm unit. The 160 μm data have an effective integration time of 120 s, and the 160 μm image reaches a sensitivity of ~ 15 mJy rms. A multiplication of 1.04 was applied to the 160 μm flux densities to color correct for galaxy SEDs. We also note that the 160 μm light leak from 1–1.6 μm is not a problem for these data, because there are no blue sources with $m_J \gtrsim 5.5$ in the field.

4. IDENTIFICATIONS AT 70 AND 160 μm

The negative K -correction at submillimeter wavelengths means that SMGs are detectable in deep SCUBA images over a wide redshift range, $1 < z < 5$ (e.g., Blain et al. 2002). However, at 70 and 160 μm , the K -correction does not compensate for the distance dimming, and the flux density of a galaxy with a given intrinsic luminosity drops steeply as a function of redshift (e.g., Lagache et al. 2005). This is reflected in the high median redshifts of the SMGs ($z \simeq 2.0$; Pope et al. 2006) compared to the 70 μm sources ($z \simeq 0.5$; M. T. Huynh et al. 2007, in preparation). Hence, the SMG and 70 μm samples are unlikely to have much overlap, and we only expect to detect the low-redshift SMGs in deep 70 μm imaging.

We examined the 70 μm image for counterparts to the SCUBA sources. To do this the 70 μm catalog positions were compared to IRAC positions of the SCUBA counterparts (Pope et al. 2006), searching within 10'' of each submillimeter counterpart. This search radius was chosen in order to take into account the typical positional uncertainties of low-S/N 70 μm and SCUBA sources added in quadrature.

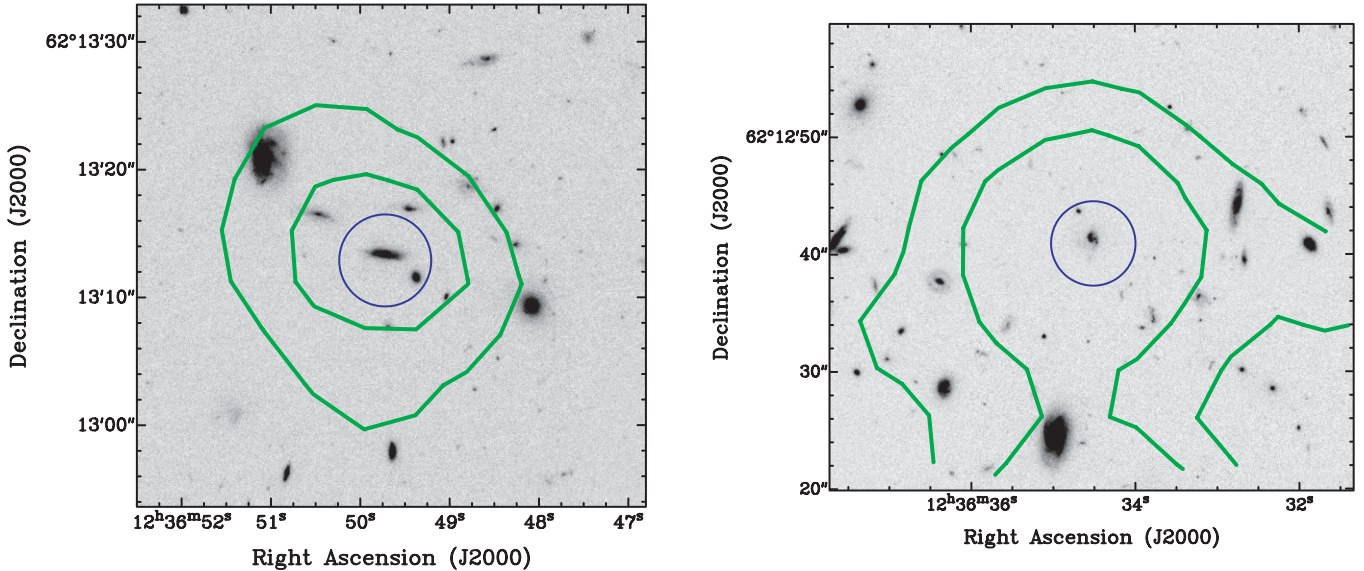


FIG. 1.— Gray-scale *HSTACS* F606W images of GN13 (*left*) and GN26 (*right*). The contours show 70 μm data, plotted at 3 and 6 σ levels. The circles indicate the Pope et al. (2006) IRAC counterpart to the SCUBA source. The images are $40'' \times 40''$ in size.

This procedure uncovered two secure identifications of SMGs at 70 μm : GN26 and GN13 (following the naming convention of Pope et al. 2005). These sources have 70 μm S/Ns of 12 and 8, respectively, and hence 70 μm positional uncertainties of about $1.3''$ and $1.5''$ (including the *Spitzer* $1''$ pointing uncertainty). The positional offset of the 70 μm source relative to the IRAC position is $0.6''$ and $0.3''$ for GN26 and GN13, respectively, which is well within the positional uncertainty. The probability that one or more 70 μm sources lies randomly within a distance θ of a SCUBA counterpart is

$$P = 1 - \exp(-\pi n \theta^2), \quad (1)$$

given a surface density n of 70 μm sources (often called the P -statistic; e.g., Downes et al. 1986). Hence, the probability of any 70 μm source lying within $1''$ of a SCUBA counterpart is 0.07%, using the 70 μm source density of 101 sources over 120 arcmin^2 , and hence the 70 μm matches to GN13 and GN26 are likely to be real.

Two more SMGs (GN12 and GN32) have a nearby 70 μm source at distances of $4.7''$ and $9.5''$, respectively. The 70 μm sources near GN12 and GN32 have IRAC and 24 μm counterparts that do not match the identifications for the SCUBA source (Pope et al. 2006). Although it is likely that some fraction of the 70 μm flux density is associated with the submillimeter galaxy, it is difficult to determine this fraction because of the other 24 μm sources in the vicinity. Using equation (1), the random probability that 2/30 SCUBA sources have a 70 μm source within a distance of $10''$ can be determined to be 28%. This is consistent with the 70 μm sources near GN12 and GN32 being random matches.

At 160 μm the only SMG detected is GN26. The beam size at 160 μm is $40''$, so 70 μm and/or SCUBA sources that are close together may be blended into one 160 μm source. Examination of the 70 μm MIPS image suggests that the 160 μm flux density of GN26 has some contribution from another 70 μm source (at $z = 0.46$) not associated with GN26. We therefore deblended GN26 with a double Gaussian fit, fixing positions to the IRAC counterparts of the two 70 μm sources that contribute to the 160 μm flux density. We find that GN26 has $S_{160} = 110 \pm 27 \text{ mJy}$, which is 60% of the flux density of the 160 μm complex. The uncer-

tainty at 160 μm is conservatively estimated to be 25%, taking into account absolute calibration, fitting errors, and deblending issues. We also examined the SED of the nearby source to check the accuracy of the deblending. The S_{70}/S_{160} ratio of the second source at $z = 0.46$ is well fit by the quiescently star-forming galaxy SED templates of Dale & Helou (2002), so the deblending at 160 μm seems reasonable.

The multiwavelength properties of the two SMGs that are detected at 70 μm (Fig. 1 and Table 1) are described in detail in Pope et al. (2006). As expected, both sources (GN26 and GN13) are in the low-redshift tail of the submillimeter redshift distribution. Furthermore, we note that these two sources are among the faintest at 850 μm in the submillimeter sample (both have $S_{850} < 2.5 \text{ mJy}$), and therefore they are not typical of the full submillimeter sample presented in Pope et al. (2006) or indeed other samples of SMGs. GN13 and GN26 have 70 μm flux densities of 6.5 and 13.9 mJy, respectively, while the full 70 μm catalog has a median flux density of 5 mJy. About 80% of the 70 μm sources have spectroscopic redshifts, and the median redshift of these sources is $z = 0.46$ (M. T. Huynh et al. 2007, in preparation). Thus, the 70 μm counterpart to GN13 is typical of the full 70 μm sample, but GN26 is unusual in that it has a bright 70 μm counterpart, and is one of only seven 70 μm sources in our sample currently confirmed to be at $z > 1$.

5. STACKING ANALYSIS

We performed a stacking analysis to derive an average 70 μm flux density for the SMG population in the GOODS-N field. To begin with, we stacked the *Spitzer* data at the positions of all SMGs, including sources with 70 μm matches or with coincident flux. For each SMG a square image $132''$ on a side (approximately seven MIPS beams) was extracted. We rotated each image by 90° with respect to the previous one before co-adding to remove any large-scale background effects. The median level of the individual extracted images was subtracted to remove any small-scale offsets and yield better background removal. Flux densities were determined using an aperture of $12''$ radius, and we applied an aperture correction of 2.0, which was calculated empirically from bright sources in the image. The aperture photometry was done after the background was subtracted from the

TABLE 1
SUMMARY OF THE PROPERTIES OF GN13, GN26, AND THE AVERAGE LOW-*z* SMG

Galaxy	R.A. (J2000.0)	Decl. (J2000.0)	S_{24} (μ Jy)	S_{70} (mJy)	S_{160} (mJy)	S_{850} (mJy)	$S_{1.4}$ (μ Jy)	z
GN13.....	12 36 49.72	62 13 12.8	371.0 ± 10.4	6.5 ± 1.3	<43	1.9 ± 0.4	45.4 ± 5.4	0.475
GN26.....	12 36 34.51	62 12 40.9	446.0 ± 5.1	13.9 ± 1.8	110 ± 27	2.2 ± 0.8	194.3 ± 10.4	1.219
Low- <i>z</i> SMG (12 sources).....	258 ± 20	1.0 ± 0.4	<22	4.0 ± 1.4	<116	1.4

NOTES.—The 70 and 160 μ m flux densities include the absolute calibration error (of order 10%). The coordinates for GN13 and GN26 are IRAC positions (Pope et al. 2006). The redshift given for the low-*z* SMGs is the median for the subsample, and the S_{850} value given for the low-*z* subsample is the weighted average. Units of right ascension are hours, minutes, and seconds, and units of declination are degrees, arcminutes, and arcseconds.

stacked images, and the results were verified by making measurements with different size sky annuli.

To estimate the expected scatter, offset stacked images were generated by randomly choosing a position in the 70 μ m image for each stacked source. Five hundred such random stacks were generated, and the uncertainty in the stacked flux density is taken to be the standard deviation of these 500 measured values.

The average 70 μ m flux density ($\langle S_{70} \rangle$) for all 30 SMGs is 2.00 ± 0.48 mJy, and hence the stacked signal is detected at over 4σ . The contribution from SMGs to the extragalactic background light (EBL) at 70 μ m can be estimated from this stacked signal by multiplying by the appropriate source density. Assuming the SMG integrated source count of 2506 ± 406 deg $^{-2}$ for $S_{850} > 2$ mJy (Coppin et al. 2006), we estimate the contribution to the 70 μ m EBL from SMGs to be 0.016 ± 0.005 MJy sr $^{-1}$. From an extrapolation of the source counts Frayer et al. (2006b) find that the total 70 μ m EBL is 0.18 MJy sr $^{-1}$, so SMGs ($S_{850} > 2$ mJy) make up about $9\% \pm 3\%$ of the 70 μ m EBL.

The 70 μ m stacked signal from all 30 SMGs is dominated by the four low-redshift sources with coincident 70 μ m flux density. To determine the average properties of the SMGs *not* detected at 70 μ m, which is more representative of the general SMG population, we also stacked the 26 sources without coincident 70 μ m flux density. This time we stacked the residual 70 μ m image, which was obtained by removing all sources brighter than 3σ at 70 μ m. Sources were removed by subtracting their fitted point-spread functions from the image. The residual image was used to obtain a better S/N in the stacked image and in the measured stacked flux density. For these 26 sources we find $\langle S_{70} \rangle = 0.70 \pm 0.27$ mJy, and so this stacked signal has an S/N of about 3.

To test whether the majority of the stacked 70 μ m flux density is from the lower redshift SMGs, we also looked at low- and high-redshift subsamples. The low-redshift subsample consists of 12 SMGs out of the 26 with $z < 2$, and the remaining 14 SMGs with $z \geq 2$ make up the high-redshift subsample. For redshift completeness we included IRAC photometric redshifts from Pope et al. (2006) for 8/26 SMGs, and these all have $z \geq 1.8$ (and estimated accuracy of $\Delta z \leq 0.4$). The aperture flux density in the central region of the high-redshift stack is 0.22 ± 0.44 mJy, while for the low-redshift stack it is more positive at 1.0 ± 0.4 mJy. This is consistent with the idea that the majority of the flux density from the full sample is coming from the lower redshift sources, although the measurements are too noisy to make a definitive statement.

Similarly, we stacked the 160 μ m image at all SMG positions, excluding the one detected source, GN26. There is no significant flux density in the stacked image, and the 3σ upper limit is 13 mJy. A stack of the 12 low-redshift SMGs gives a 3σ upper limit at 160 μ m of 22 mJy.

To study the FIR properties of SMGs we could use the average flux densities of the full sample of SMGs. However, the stacked

70 μ m flux density from the separate high- and low-*z* subsamples clearly show that most of the signal is coming from $z < 2$ sources (as expected from the *K*-correction). We therefore limit our analyses to the average properties of the low-*z* subsample in the following sections.

6. INFRARED COLORS

The average IR colors, S_{70}/S_{850} and S_{70}/S_{24} , are shown in Figure 2 as a function of redshift. GN26, at $z \sim 1.5$, is consistent with a more active Dale & Helou (2002, hereafter DH02) model, with dust intensity index $\gamma = 1.5$, whereas GN13 has cooler colors, corresponding to $\gamma = 2.5$. In the DH02 models γ defines the amount of dust as a function of heating intensity (Dale et al. 2001):

$$dM(U) \propto U^{-\gamma} dU,$$

where $M(U)$ is the dust mass heated by a radiation field of intensity U . These γ -values span the range expected for IR-luminous

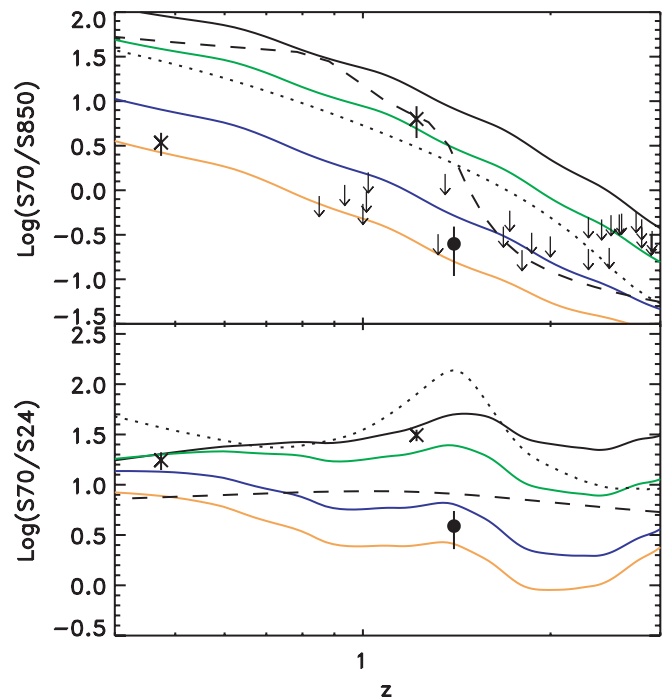


FIG. 2.—Top: S_{70}/S_{850} colors of the DH02 models as a function of redshift. From top to bottom, the solid lines are $\gamma = 1, 1.5, 2,$ and 2.5 . The dotted line marks the ratio from an Arp 220 SED, while the dashed line is the ratio for Mrk 231. The crosses mark the SMGs GN13 and GN26, which are detected at 70 μ m. Other SMGs are shown as 3σ upper limits. The circles denote the average ratios from the stacked analysis of the low-*z* subsample at $\langle z \rangle = 1.4$. Bottom: S_{70}/S_{24} colors of the DH02 models. Lines and symbols same as in the top panel.

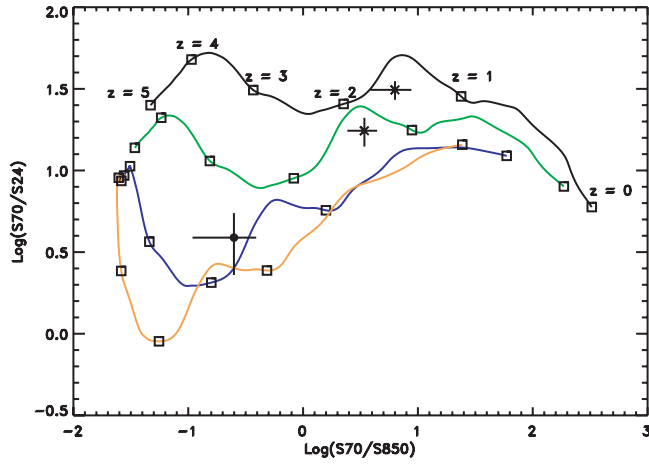


FIG. 3.— Plot of S_{70}/S_{24} vs. S_{70}/S_{850} colors compared with the DH02 models. For each model the squares mark redshift 0, 1, 2, 3, 4, and 5, from right to left. The models from top to bottom are for $\gamma = 1, 1.5, 2,$ and 2.5 . The crosses mark the SMGs GN13 and GN26, which are detected at 70 μm . The circle marks the average for the low- z SMG subsample.

galaxies—a low value around 1 implies a high contribution from photodissociation regions in an actively star-forming galaxy, while a significantly higher value represents the cirrus-dominated interstellar medium of a more quiescent or cooler galaxy.

The IR colors of the average low- z SMG are consistent with $\gamma \simeq 2$ – 2.5 DH02 SEDs. The average S_{70}/S_{850} ratio of SMGs from the stacking analysis indicates that the SMGs are relatively cool galaxies for their high IR luminosities, which is consistent with Pope et al. (2006). We also calculated upper limits to the S_{70}/S_{850} ratio for SMGs *not* detected individually at 70 μm (see Fig. 2). The lower redshift SMGs are clearly inconsistent with lower values of γ . For the higher redshift sources we expect much lower S_{70}/S_{850} ratios, but with the current observational limits these sources can still be actively star forming.

For GN13, Figure 2 shows that the S_{70}/S_{24} ratio is that of an actively star-forming galaxy, with $\gamma \simeq 1$ – 1.5 , while the S_{70}/S_{850} ratio indicates it is a cooler galaxy. This may be due to broad silicate absorption falling into the 24 μm band; the S_{70}/S_{24} ratio can be strongly affected by PAH features and silicate absorption, which are not fully accounted for in the models.

We find that the colors of GN26 are consistent with DH02 models with $\gamma = 1$ and $z \simeq 1$ – 2 (Fig. 3). The colors of GN13 place it at $z = 1$ – 2 if a $\gamma = 1.5$ model is assumed (Fig. 3). However, GN13 is at $z = 0.475$, and so this SMG has a warmer S_{70}/S_{24} ratio than that suggested by its S_{70}/S_{850} ratio, as mentioned earlier.

The average colors of low- z SMGs are also plotted in Figure 3. We find that the average IR colors are best represented with a DH02 model having $\gamma \simeq 2$ – 2.5 at $z = 1$ – 2 . This is consistent with the median redshift of the low- z SMG subsample and suggests the color-color plot can be used as a crude redshift indicator.

7. SPECTRAL ENERGY DISTRIBUTION

The FIR photometry at 70 and 160 μm provides valuable data points for constraining the FIR peak. Combined with the 850 μm observations, the photometry spans both sides of the peak. Previous estimates of the SED of SMGs have relied on extrapolating the MIR or radio to fit the FIR peak—at the redshifts of SMGs, the MIR can be affected by complex emission and absorption features, so this method may not be reliable.

We fit a variety of models to the data. These include four DH02 models with $\gamma = 1, 1.5, 2,$ and 2.5 , as well as the Chary & Elbaz (2001, hereafter CE01) SEDs, which are templates derived from ISOCAM, *IRAS*, and SCUBA data of nearby galaxies. The CE01 models have luminosity-dependent shapes, but since the local luminosity-temperature relation found for nearby galaxies may not hold for high- z SMGs (e.g., Pope et al. 2006), we fit CE01 models allowing them to scale arbitrarily in luminosity.

For GN13 and for the low- z SMG subsample, we constrain the fit with the 70 and 850 μm observations only, since they are not detected at 160 μm (although the 160 μm data provide a useful upper limit). For GN26, the 70, 160, and 850 μm observations are all used to constrain the fit. We summarize the fitting results in Table 2, while Figures 4 and 5 show the best-fit SEDs for GN13, GN26, and the average low- z SMG. Fitting CE01 SEDs without allowing the luminosity to vary freely results in relatively poor fits, so we exclude these from the table. This confirms the Pope et al. (2006) result that the local luminosity-temperature relationship does not hold for SMGs. For each best-fit SED the total L_{IR} (between 8 and 1000 μm) was calculated and given in Table 2. Uncertainties in the luminosity were derived by scaling the best-fit SED until the minimum χ^2 value exceeded the 68% ($\pm 1 \sigma$) confidence interval.

The models provide good fits to the 70 and 850 μm data for GN13 and for the low- z average SMG, but they do not typically fit the 24 μm (observed) data point, although it has been shown that the 24 μm flux density can often be fit with additional extinction (Pope et al. 2006). The models do not provide a similarly good fit in the FIR for GN26; the 70 and 850 μm data points of GN26 are well fit, but the 160 μm measurement is underestimated by the models. Hence, the luminosity for GN26 is probably higher than given by these models. Nevertheless, our derived IR luminosity for GN26 is 3 times greater than that estimated by Pope et al. (2006) from fitting SEDs to 24 μm , 850 μm , and 1.4 GHz radio data. It is possible that there are further deblending issues at 160 μm for GN26 (even although we have already divided the total 160 μm flux density between the two 70 μm sources in the area). This demonstrates the power of 160 μm photometry in constraining the total IR luminosity of galaxies, but shows that higher resolution is required to study such faint sources individually.

The SMGs have high luminosities, but their FIR spectral shape is different from local ULIRGs of the same luminosity. We find that the average low- z SMG has a total IR luminosity of about $8.0 \times 10^{11} L_{\odot}$. This is a factor $\simeq 2$ less than the median

TABLE 2
SUMMARY OF THE BEST-FIT SEDS AND THE CALCULATED TOTAL L_{IR}

Galaxy	Best-fit DH02	DH02 L_{IR} (L_{\odot})	Luminosity-scaled CE01 L_{IR} (L_{\odot})
GN13.....	$\gamma = 2.5$	$(2.5 \pm 0.3) \times 10^{11}$	$(1.8 \pm 0.2) \times 10^{11}$
GN26.....	$\gamma = 1.5$	$(4.5 \pm 0.7) \times 10^{12}$	$(5.0 \pm 0.7) \times 10^{12}$
Low- z SMG (12 sources).....	$\gamma = 2.5$	$(9.0 \pm 2.5) \times 10^{11}$	$(8.0 \pm 2.2) \times 10^{11}$

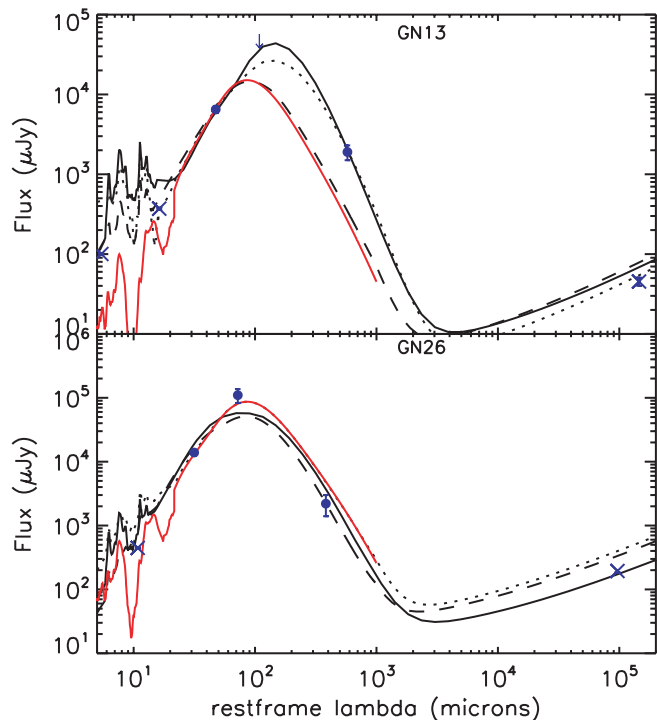


FIG. 4.—SEDs of GN13 and GN26. The observed *Spitzer* and SCUBA data are plotted at rest-frame wavelengths. The best-fit DH02 model is plotted as a solid black line, while the dashed line is the best-fit CE01 luminosity-dependent SED, and the dotted line is the best-fit CE01 SED with luminosity allowed to vary. The best-fit Arp 220 SED is also shown as the solid red line. The fits were constrained using only the 70 and 850 μm data for GN13, and with the addition of the 160 μm data point for GN26.

SMG luminosity found by Pope et al. (2006) and Chapman et al. (2005) for their SMGs with $z < 2$. The reason that our calculated SMG luminosities are low compared to previous results is because our best-fit SEDs are cooler. The average SMG is best fit by a quiescent DH02 model with $\gamma \simeq 2.5$, or with CE01 SED templates of normal spiral galaxies scaled up by a factor $\simeq 300$, with a rest-frame peak at about 150 μm (i.e., $T \simeq 20$ K). Local ULIRGs of the same luminosity as the SMGs are therefore not the best spectral templates for this sample.

Several recent studies have relied on the MIR data (at 24 μm in particular) to derive luminosities and SED fits (e.g., Pérez-González et al. 2005; Le Floc’h et al. 2005). The 24 μm flux density was used in SED fitting of SMGs by Pope et al. (2006), who found that the typical SMG peaks at about 100 μm (corresponding to about 29 K). If the 24 μm data point is included in the fitting of GN13 along with the 70 and 850 μm data, we find the best-fit DH02 SED peaks at shorter wavelength, corresponding to warmer dust temperatures, and the total IR luminosity is decreased by a factor of about 2. There is no significant difference in the CE01 fits to GN13 with and without the 24 μm data point. For GN26 we find the 24 μm data point makes no significant difference to the best-fit DH02 SED, while the best-fit CE01 model is slightly warmer and 3 times less luminous. The fit to the average SMG including the 24 μm data point is warmer than that with only the longer wavelength data, and the best-fit DH02 and CE01 SEDs are about 2 times more luminous. At the median redshift of the average low- z SMG, $\langle z \rangle = 1.4$, PAH and silicate features fall into the 24 μm band, and our fit here is driven by these features in the model SEDs. The DH02 and CE01 SEDs certainly contain PAH features, but it is not clear whether SMGs at this redshift have strong or weak PAH features, if any. Therefore, we would

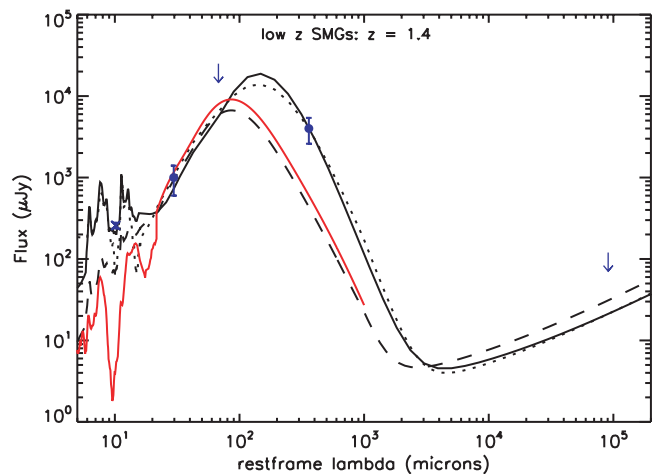


FIG. 5.—SED of the average low- z SMG. The observed *Spitzer* and SCUBA data are plotted at rest-frame wavelengths, and the curves are best-fit DH02 model (solid black line), best-fit CE01 luminosity-dependent SED (dashed line), best-fit CE01 SED with luminosity allowed to vary (dotted line), and best-fit Arp 220 SED (solid red line). The fits were constrained using the 70 and 850 μm data only, as described in the text.

argue that the fit to the 850 and 70 μm flux densities alone gives a more reliable result for the average SMG total luminosity, at least for the moment, until we learn more about the MIR spectra of SMGs.

8. DUST TEMPERATURES AND MASSES

As a phenomenological alternative, we also adopt a modified blackbody SED model to fit the temperature of these SMGs. The SED is described by $f_\nu \propto \nu^\beta B_\nu$, where $B_\nu(\nu, T)$ is the blackbody function for dust of temperature T and β is the dust emissivity index. The MIR is approximated as a power law of the form $f_\nu \propto \nu^{-\alpha}$ and smoothly matches $\nu^\beta B_\nu$ at longer wavelengths (Blain et al. 2003). Although this simple phenomenological model cannot describe the full complex dust properties of a galaxy, it can provide a good description of the general behavior of the SED. The range of parameters we consider is $15 \text{ K} < T < 90 \text{ K}$ and $1 < \alpha < 4$, which is representative of galaxies ranging from normal spirals to active galactic nuclei (AGNs). We set $\beta \equiv 1.5$ for our model fits, which is the value found for dust in the Galactic plane (Masi et al. 1995), and a typical value for well-studied nearby galaxies (Dunne et al. 2000).

We fit for T and α using the 70 and 850 μm data points for GN13 and the average low- z SMG, but also include the 160 μm detection for GN26. The results are summarized in Table 3. When fitting only two data points (and allowing the normalization to also be free) there is a strong degeneracy between α and T (which would be complete except for the boundaries of the parameter ranges)—so the fit parameters must be interpreted with caution. In the case of GN13, the full range of α is allowed by the 70 and 850 μm data, with low values of α corresponding to low values of T . Because of the additional 160 μm data point, the parameters are better constrained for GN26, with $T \simeq 45$ K and $\alpha \simeq 3.5$ being preferred.

For the average SMG, the 70 and 850 μm flux densities alone cannot break the T and α degeneracy—a very low temperature of 15 K is allowed for $\alpha \simeq 1.0$, while $T \simeq 33$ K for $\alpha \simeq 4.0$. In a sample of 73 radio-detected SMGs the average S_{450}/S_{850} ratio is measured to be 5.0 ± 2.3 (Chapman et al. 2005), while 15 SMGs from this same sample have been detected with the

TABLE 3
ALLOWABLE MODEL PARAMETERS FOR A SIMPLE MODIFIED
BLACKBODY SED

Galaxy	T (K)	α
GN13.....	34–50	1.0–4.0
GN26.....	44–48	3.0–4.0
Low- z SMG (12 sources).....	21–33	1.6–4.0

NOTES.—The range in T and α indicates the models that fit within the 1σ limit of the 70, 160, and 850 μm observations. The dust emissivity parameter, β , is assumed to be 1.5.

second-generation Submillimeter High Angular Resolution Camera (SHARC-II; Kovacs et al. 2006), and they have an average S_{350}/S_{850} ratio of 4.0 ± 1.3 . We find that models with $\alpha < 1.6$ are inconsistent with these ratios. This implies that the allowed models for the average SMG have $21\text{ K} < T < 33\text{ K}$ and $1.6 < \alpha < 4.0$, where the low values of T require low α . This shows that the low- z SMGs have relatively cool dust temperatures.

The best-fit dust temperatures of 21–33 K are consistent with those values previously derived for SMGs (e.g., Pope et al. 2006). Chapman et al. (2005) and Kovacs et al. (2006) suggested average temperatures close to the upper end of our acceptable range. This implies that the average low- z SMG in our sample has a relatively steep MIR SED, since our model fits with $T \simeq 30\text{ K}$ require $\alpha \simeq 3$. This suggests that the SMGs are star-forming galaxies, because large α implies cool MIR colors, which are inconsistent with AGN-dominated sources.

Assuming that the submillimeter light is thermal emission from dust that is optically thin at $\lambda_{\text{rest}} \sim 200\ \mu\text{m}$, with a single dust temperature T , the dust mass M_d is given by

$$M_d = \frac{S_{850} D_L^2}{(1+z)\kappa_d(\nu_{\text{rest}})B_\nu(\nu_{\text{rest}}, T)} \quad (2)$$

(e.g., McMahon et al. 1994), where D_L is the cosmological luminosity distance at redshift z and the dust absorption coefficient κ is uncertain, even in the local universe. We take a κ -value of $0.077 \pm 0.030\ \text{m}^2\ \text{kg}^{-1}$ (Hughes et al. 1993), converting it to rest-frame frequency ν_{rest} with

$$\kappa_d(\nu_{\text{rest}}) = 0.077 \left(\frac{\nu_{\text{rest}}}{350\ \text{GHz}} \right)^\beta. \quad (3)$$

Here we again assume that the dust emissivity index β is fixed at 1.5.

The range of allowable dust masses are calculated from the range of temperatures in Table 3. The dust mass calculated from equation (2) is $(1.0\text{--}1.6) \times 10^8$ and $(2.2\text{--}2.5) \times 10^8\ M_\odot$ for GN13 and GN26, respectively, while the dust mass found for the average low- z SMG is $(1.1\text{--}2.6) \times 10^9\ M_\odot$. This does not take into account the uncertainties in κ and S_{850} ; the dust mass uncertainty is about 50% when these are added in quadrature. These dust masses are consistent, within uncertainties, with the molecular gas mass derived from CO observations (e.g., Frayer et al. 1998, 1999; Neri et al. 2003; Greve et al. 2005), assuming a typical galactic gas mass-to-dust mass ratio $M_g/M_d \simeq 100$ (e.g., Hildebrand 1983).

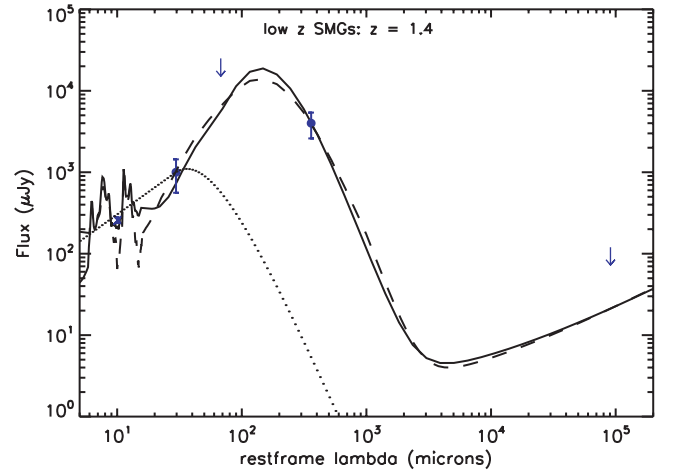


FIG. 6.—Best-fit SEDs for the low- z SMG subsample. The solid line is the DH02 model, and the dashed line is the best-fit CE01 model (allowing the luminosity to float freely). The dotted line shows the AGN contribution allowed before all the CE01 models fail at the 1σ level. Symbols same as in Fig. 5.

9. FIR-RADIO CORRELATION

Our sample can be used to test the FIR-radio correlation in submillimeter galaxies. The FIR-radio correlation is often expressed as (e.g., Yun et al. 2001)

$$q \equiv \log \left(\frac{\text{FIR}}{3.75 \times 10^{12}\ \text{W m}^{-2}} \right) - \log \left(\frac{S_{1.4}}{\text{W m}^{-2}\ \text{Hz}^{-1}} \right), \quad (4)$$

where FIR refers to the flux between 40 and 120 μm . The observed local value is $q = 2.34 \pm 0.3$ (Yun et al. 2001). We use the best-fit DH02 models to derive the conversion from $L_{40\text{--}120}$ to $L_{8\text{--}1000}$, which is 2.0 and 1.6 for GN13 and GN26, respectively. Based on their L_{IR} (Table 2), we find q parameters of $2.5^{+0.3}_{-0.1}$ and $2.4^{+0.1}_{-0.1}$ for GN13 and GN26, respectively. These values are consistent with the local value of q , suggesting that these two sources follow the local FIR-radio correlation.

10. CONTRIBUTION FROM ACTIVE GALACTIC NUCLEI

As mentioned in § 8, the inferred high values of α suggest that AGNs do not dominate the bolometric luminosity in our sample of SMGs. To quantify the contribution of AGNs to the IR luminosity of SMGs, we adopt the simple modified blackbody approach as described in § 8. For our AGN model we use $\beta = 1.5$, $T = 90\text{ K}$, and $\alpha = 1.1$, as found for the xFSL AGN population (Frayer et al. 2006a). We subtract this AGN component from the observed 70 and 850 μm flux densities of the average SMG, and then repeat the fitting procedure with the DH02 and CE01 models, increasing the AGN component until the best-fit χ^2 value exceeds the previous minimum by 1σ . This allows us to estimate the maximum AGN contribution to the FIR luminosity, with the results shown in Figure 6.

It could be argued that the MIR wave band is the best discriminator of AGNs, and therefore we should be focusing on the 24 μm data point (e.g., Sajina et al. 2005). However, we are here calculating the percentage contribution of AGNs to the L_{IR} , which is dominated by the FIR peak, and the contribution from AGN emission in the MIR is only a very small proportion of the total IR luminosity.

For the average low- z SMG, an AGN that contributes up to 14% of the IR luminosity is allowed, using only the previous best-fit CE01 SED model. If all CE01 models are used in the refitting,

an AGN component of up to 23% contribution is allowed. Together these fitting procedures imply that the average (low- z subsample) SMG is dominated by a starburst. This is consistent with X-ray studies, which find that AGNs contribute on average 10% to the IR luminosity of SMGs (Alexander et al. 2005).

For the 70 μm -detected SMGs, GN13 and GN26, we find that 32% and 21%, respectively, of the total IR luminosity can be attributed to an AGN from the same analysis applied to the best-fit templates. However, if the whole suite of CE01 SEDs are used, a larger proportion of the IR luminosity can be subtracted off the observed data points, with lower luminosity CE01 models still fitting. This shows that with the current data a low-luminosity starburst model from CE01 with an additional dominant AGN component is indistinguishable from a high-luminosity CE01 ULIRG model, and that further photometry (or spectroscopy) is needed.

Another method to estimate the AGN contribution is to make use of the 24 μm data. Here, we consider the extreme case in which all the 24 μm flux density is due to an AGN and determine its contribution to the total IR luminosity. For GN13 and GN26 such an AGN would contribute 11% and 5%, respectively, to the total IR luminosity, assuming the $T = 90$ K, $\alpha = 1.1$ AGN model used above, and the CE01 best-fit SEDs. For the average low- z SMG, 21% of the total IR luminosity could be attributed to an AGN in this extreme case. This again supports the hypothesis that SMGs are dominated by star formation processes.

11. CONCLUDING REMARKS

We have presented 70 μm properties of submillimeter galaxies in the GOODS-N field. Out of 30 SMGs (with $S_{850} > 1.7$ mJy) in the overlap region of this field, two are detected at relatively high significance in ultradeep (~ 0.6 mJy rms) 70 μm imaging. Both of these detected SMGs lie at relatively low redshift. One SMG, GN26 at redshift $z = 1.2$, has IR colors that indicate it is actively star forming. The second SMG, GN13 ($z = 0.47$), has IR colors similar to normal spirals, but with a much higher luminosity. We confirm that these two SMGs detected at 70 μm follow the locally derived FIR-radio correlation.

To determine the average properties of SMGs (most of which lie at $z > 2$ and are not detected individually at 70 μm), we performed a stacking analysis and find that the average SMG has a 70 μm flux density of 0.70 ± 0.27 mJy. Most of the 70 μm flux density is coming from the lower redshift SMGs, however. We analyzed the average properties of 12 SMGs with $z < 2$, which have a stacked 70 μm flux density of 1.0 ± 0.4 mJy. From a stack

of all 30 SMGs in the ultradeep 70 μm image, we find that the contribution of SMGs (with $S_{850} > 2$ mJy) to the total extragalactic background light at 70 μm is $9\% \pm 3\%$.

The average low- z SMG ($\langle z \rangle = 1.4$) has cool IR colors and an FIR SED that is best fit by a scaled-up (about 300 times) normal spiral galaxy. We also found that an AGN contributes less than 23% of the total IR luminosity in SMGs.

We find that the average low- z SMG has an IR luminosity, L_{8-1000} , of $8.0(\pm 2.2) \times 10^{11} L_{\odot}$. The average low- z SMG therefore has a star formation rate of $135 \pm 35 M_{\odot} \text{ yr}^{-1}$, using the relationship between SFR and IR luminosity for starburst galaxies given by Kennicutt (1998). GN13 and GN26 have star formation rates of 30 ± 10 and $800 \pm 270 M_{\odot} \text{ yr}^{-1}$, respectively. The median IR luminosity of $z < 2$ SMGs in Chapman et al. (2005) is twice the value we find for our average low- z SMG, suggesting that theirs may have been an overestimate, suffering from lack of FIR data.

The next-generation submillimeter bolometer, SCUBA-2, will come online in 2007 (Holland et al. 2006), and it is expected to yield a major improvement at 450 μm , where it should reach a confusion limit of ~ 1 mJy (5σ). This depth is well matched to that of deep *Spitzer* 70 μm imaging and should provide much more overlap than the 850 μm -selected sources. In addition, SCUBA-2 will produce much larger samples of fainter 850 μm sources, much like the two 70 μm -detected submillimeter sources in this study, and therefore 70 μm data will be a valuable addition to understanding their SEDs. Also in the near future, the *Herschel Space Observatory* will produce confusion-limited images across the wavelength range 75–500 μm . *Herschel* will therefore enable detailed study of the FIR SEDs of large samples of SMGs, which we have shown here to be feasible for a subset of SMGs using *Spitzer*.

We thank the anonymous referee for helpful comments that improved this paper. M. T. H. would like to thank Anna Sajina for helpful discussions. A. P. and D. S. acknowledge support from the Natural Sciences and Engineering Research Council of Canada and the Canadian Space Agency. This work is based in part on observations made with the *Spitzer Space Telescope*, which is operated by the Jet Propulsion Laboratory, California Institute of Technology, under a contract with NASA. Support for this work was provided by NASA through an award issued by JPL/Caltech.

REFERENCES

- Alexander, D. M., Bauer, F. E., Chapman, S. C., Smail, I., Blain, A. W., Brandt, W. N., & Ivison, R. J. 2005, *ApJ*, 632, 736
- Barger, A. J., Cowie, L. L., & Richards, E. A. 2000, *AJ*, 119, 2092
- Barger, A. J., Cowie, L. L., Sanders, D. B., Fulton, E., Taniguchi, Y., Sato, Y., Kawara, K., & Okuda, H. 1998, *Nature*, 394, 248
- Blain, A. W., Barnard, V. E., & Chapman, S. C. 2003, *MNRAS*, 338, 733
- Blain, A. W., Smail, I., Ivison, R. J., Kneib, J.-P., & Frayer, D. T. 2002, *Phys. Rep.*, 369, 111
- Borys, C., Chapman, S. C., Halpern, M., & Scott, D. 2002, *MNRAS*, 330, L63
- Borys, C., et al. 2003, *MNRAS*, 344, 385
- Chapman, S. C., Blain, A. W., Smail, I., & Ivison, R. J. 2005, *ApJ*, 622, 772
- Chapman, S. C., Lewis, G. F., Scott, D., Borys, C., & Richards, E. 2002, *ApJ*, 570, 557
- Chapman, S. C., Smail, I., Blain, A. W., & Ivison, R. J. 2004, *ApJ*, 614, 671
- Chary, R., & Elbaz, D. 2001, *ApJ*, 556, 562 (CE01)
- Coppin, K., Halpern, M., Scott, D., Borys, C., & Chapman, S. 2005, *MNRAS*, 357, 1022
- Coppin, K., et al. 2006, *MNRAS*, 372, 1621
- Dale, D. A., & Helou, G. 2002, *ApJ*, 576, 159 (DH02)
- Dale, D. A., Helou, G., Contursi, A., Silbermann, N. A., & Kolhatkar, S. 2001, *ApJ*, 549, 215
- Dole, H., et al. 2004, *ApJS*, 154, 87
- Downes, A. J. B., Peacock, J. A., Savage, A., & Carrie, D. R. 1986, *MNRAS*, 218, 31
- Dunne, L., Eales, S., Edmunds, M., Ivison, R., Alexander, P., & Clements, D. L. 2000, *MNRAS*, 315, 115
- Frayer, D. T., Ivison, R. J., Scoville, N. Z., Yun, M., Evans, A. S., Smail, I., Blain, A. W., & Kneib, J.-P. 1998, *ApJ*, 506, L7
- Frayer, D. T., et al. 1999, *ApJ*, 514, L13
- . 2006a, *AJ*, 131, 250
- . 2006b, *ApJ*, 647, L9
- Gordon, K. D., et al. 2005, *PASP*, 117, 503
- Greve, T. R., Ivison, R. J., Bertoldi, F., Stevens, J. A., Dunlop, J. S., Lutz, D., & Carilli, C. L. 2004, *MNRAS*, 354, 779
- Greve, T. R., et al. 2005, *MNRAS*, 359, 1165
- Hildebrand, R. H. 1983, *QJRAS*, 24, 267
- Holland, W. S., et al. 1999, *MNRAS*, 303, 659
- . 2006, *Proc. SPIE*, 6275, 62751E

- Hughes, D. H., Robson, E. I., Dunlop, J. S., & Gear, W. K. 1993, MNRAS, 263, 607
- Hughes, D. H., et al. 1998, Nature, 394, 241
- Iverson, R. J., Smail, I., Barger, A. J., Kneib, J.-P., Blain, A. W., Owen, F. N., Kerr, T. H., & Cowie, L. L. 2000, MNRAS, 315, 209
- Kennicutt, R. C. 1998, ARA&A, 36, 189
- Klaas, U., Haas, M., Heinrichsen, I., & Schulz, B. 1997, A&A, 325, L21
- Kovacs, A., et al. 2006, ApJ, 650, 592
- Kreysa, E., et al. 1998, Proc. SPIE, 3357, 319
- Lagache, G., Puget, J.-L., & Dole, H. 2005, ARA&A, 43, 727
- Le Floc'h, E., et al. 2005, ApJ, 632, 169
- Masi, S., et al. 1995, ApJ, 452, 253
- McMahon, R. G., Omont, A., Bergeron, J., Kreysa, E., & Haslam, C. G. T. 1994, MNRAS, 267, L9
- Neri, R., et al. 2003, ApJ, 597, L113
- Pérez-González, P. G., et al. 2005, ApJ, 630, 82
- Pope, A., Borys, C., Scott, D., Conselice, C., Dickinson, M., & Mobasher, B. 2005, MNRAS, 358, 149
- Pope, A., et al. 2006, MNRAS, 370, 1185
- Sajina, A., Lacy, M., & Scott, D. 2005, ApJ, 621, 256
- Sajina, A., Scott, D., Dennefeld, M., Dole, H., Lacy, M., & Lagache, G. 2006, MNRAS, 369, 939
- Smail, I., Ivison, R. J., & Blain, A. W. 1997, ApJ, 490, L5
- Webb, T. M., et al. 2003, ApJ, 587, 41
- Yun, M. S., Reddy, N. A., & Condon, J. J. 2001, ApJ, 554, 803